Experimental investigation on the effect of natural fire exposure on the post-fire behaviour of reinforced concrete beams using electric radiant panel

Balša Jovanović[1], Robby Caspeele[2], Edwin Reynders[3], Geert Lombaert[4], Florian Put[5], Andrea Lucherini[6], Ruben Van Coile[7]

Abstract

In this study, the effects of natural fire exposure on the post-fire behaviour of concrete beams are investigated. The study is based on laboratory tests where three reinforced concrete beams were

[1]**Corresponding author**

PhD student, Department of Structural Engineering and Building Materials, Ghent University, Belgium

Department of Civil Engineering, Structural Mechanics Section, KU Leuven, Belgium,

e-mail: Balsa.Jovanovic@ugent.be, ORCID: https://orcid.org/ 0000-0001-5200-5848

[2] **Professor, Department of Structural Engineering and Building Materials, Ghent University, Belgium,**

e-mail: Robby.Caspeele@ugent.be, ORCID: https://orcid.org/0000-0003-4074-7478

[3] **Professor, Department of Civil Engineering, Structural Mechanics Section, KU Leuven, Belgium,**

e-mail: Edwin.Reynders@kuleuven.be, ORCID: https://orcid.org/ 0000-0002-1042-0282

[4] **Professor, Department of Civil Engineering, Structural Mechanics Section, KU Leuven, Belgium,**

e-mail: Geert.Lombaert@kuleuven.be, ORCID: https://orcid.org/ 0000-0002-9273-3038

[5] **PhD student, Department of Structural Engineering and Building Materials, Ghent University, Belgium**

e-mail: Florian.Put@UGent.be, ORCID: https://orcid.org/0000-0002-4522-9015

[6] **PhD, Senior Researcher, Slovenian National Building and Civil Engineering Institute (ZAG), Slovenia**

e-mail: Andrea.Lucherini@zag.si, ORCID: https://orcid.org/0000-0001-8738-1018

[7] **Professor, Department of Structural Engineering and Building Materials, Ghent University, Belgium,**

e-mail: Ruben.VanCoile@ugent.be, ORCID: https://orcid.org/ 0000-0002-9715-6786

subjected to fire exposure using an electric radiant panel. This panel enables a precise application of radiative heat exposure closely mimicking natural fire exposure in a safe manner. During the test, the deflections, deformations and temperature changes are measured for all three concrete beams. Additionally, Finite Element Modeling (FEM) is applied to supplement these tests, demonstrating the performance of existing structural fire engineering calculation tools in evaluating the burnout performance of concrete beams.

The results of the tests show that the electric radiant panel provide a novel approach for fire simulation which is effective in replicating natural fire conditions, by applying the heat flux as specified in the Eurocode Parametric Fire Curve in a highly controlled manner. The uniformity of the temperature field measured inside the beams and the consistent deformations observed during the heat exposure across all three tests underscores the accuracy of the fire simulation. Furthermore, post-fire assessments reveal that while the exposed beams suffered some reduction in load-bearing capacity, they retained a significant portion of their original strength that was consistent across all three beams.

The numerical simulations conducted in this study demonstrate a high level of accuracy in predicting the behaviour of the concrete beams during fire exposure. These simulations effectively mirrored the experimental results, validating that they are a valuable tool for assessing concrete structures' performance in fire scenarios.

1. Introduction

Due to their thermal and mechanical properties, concrete members are highly resistant to fire exposure and in a large number of cases survive fire exposure without collapsing [1], [2]. Understanding the behaviour of concrete structures after fire exposure is essential for several reasons. First and foremost, post-fire assessment provides valuable insights into the extent of damage incurred during a fire. Additionally, it enables engineers and researchers to evaluate the residual load-carrying capacity of such structures in the aftermath of a fire event. This knowledge is crucial for determining whether a structure remains safe for occupancy or requires immediate repair or rehabilitation. This information

is key in guiding structural repair and retrofitting efforts, ultimately contributing to the overall safety and longevity of concrete buildings and infrastructure [3].

Fires not only subject structures to elevated temperatures but also induce complex thermal and mechanical interactions within the materials. These interactions can lead to changes in material properties, microcracking, and even structural deformations, all of which have direct implications on the safety and performance of concrete structures [4].

In order to accurately predict and understand the post-fire behaviour of concrete members, their behaviour during the fire must also be known and understood. One approach to achieve this is through experimental testing, where structural members are tested at full scale while being exposed to the entire fire progression, including both the heating and cooling phases. In order to properly understand the residual behaviour for research purposes, structural members can be tested at full scale while exposed to the whole progression of the fire including both the heating and the cooling phase. While large-scale tests provide valuable insights into fire-induced damage, they often come with significant financial and logistical efforts. Additionally, due to the difficulty of controlling the exact fire exposure, the repeatability of these tests can be difficult to achieve. Moreover, accurately following prescribed cooling phases in these tests can be inherently challenging, potentially limiting their practicality. The importance of the cooling phase and the difficulties in employing it in large-scale tests have been demonstrated in [5].

For those reasons, there has been an emerging trend of developing methods to directly control the thermal boundary conditions to the test specimens. One example is the H-TRIS system [6] which employs a gas-powered radiant panel that can precisely control the applied heat flux to the sample by adjusting the distance between the panel and the sample. In the work presented here, a similar technique employing an electric intensity-controlled radiant panel is used.

An experimental program was developed which focuses on the assessment of the behaviour of concrete beams after exposure to fire. The experiments aim to replicate fire exposure through

controlled heating and loading conditions. Four identical concrete beams are considered, including one beam serving as a reference which is not exposed to the fire. These tests are designed to evaluate the beams' structural response, including deflections, deformations, and temperature distributions, during and after the simulated fire exposure. The comprehensive instrumentation system employed in this study includes load cells, LVDTs, thermocouples, and Digital Image Correlation (DIC), enabling precise data collection and analysis. In addition to the experimental program, finite element modelling (FEM) is used to simulate the structural response of concrete beams. This added dimension demonstrates the ability of current modelling approaches, particularly in simulating fires with cooling phases. The inclusion of FEM provides a more nuanced examination of structural responses during the fire exposure, complementing the insights gained from the experimental phase. In the following, the experimental program and results are presented in sections 2 and 3. Section 4 elaborates on the numerical modelling

2. Experimental program

Four identical concrete beams are tested (B1, B2, B3 and BR). Beams B1, B2 and B3 are exposed to the heating regime simulating natural fire exposure and beam BR is kept as a reference and is not exposed to the heating. The testing consists of three stages. The first stage is the mechanical loading and unloading until the “serviceability” load (in this case 67% of the beams’ design bending capacity). This stage is conducted to make a distinction between cracks induced by regular damage and additional accidental fire damage. These tests are conducted to assess the damage level of the beams prior to the fire exposure. This is done to allow for a subsequent comparison with the damage level assessed post-fire. All four beams are subjected to this first loading stage. The second stage is the heating stage where thermal loading is imposed using an electrical radiant panel, while the mechanical load is kept constant. Finally, the third stage is conducted to determine the residual bending capacity of all four beams through a four-point flexural bending test.

2.1. Beam description

All four beams utilized in the experimental campaign are identical in terms of their dimensions and are cast from the same batch of concrete. The constituents of the concrete mix are listed in Table 1. These beams have a length of 3.8 meters, a cross-sectional height of 0.29 m, and a width of 0.2 m. Each beam is reinforced with a total of 5 steel rebars, each having a diameter of 16 mm. Among these rebars, 3 are positioned in the tensioned zone of the beam, while the remaining 2 are placed in the compressed zone. A concrete cover of 20 mm (from all edges) is maintained for all 5 bars. The selection of this relatively low cover thickness compared to the usual design was deliberate, aiming at the investigation of concrete beams that are more susceptible to fire exposure. To enhance the structural integrity, 8 mm stirrups are employed as shear reinforcement, spaced at 20 cm intervals along the length of the beams. The tested beams are made of C30/37 concrete with siliceous aggregate and B500B steel is used for the reinforcement. The design moment capacity is equal to 61.6 kNm according to the calculation approach presented in [7].

Table 1 Concrete mix constituents

Materials	**Weight** $[\mathbf{kg/m^3}]$	**Mixing ratios [-]**
Cement	330	1.00
Coarse aggregate (4/20)	995	3.02
River sand (0/2)	453	1.37
Crushed sand (0/4)	371	1.12
Water	189	0.55

The mechanical properties of the concrete are assessed after 28 days on 3 standard cubes (150 mm x 150 mm x 150 mm) and 3 standard cylinders (diameter 150 mm, height 300 mm). The samples were stored at the same ambient conditions as the beams themselves. The compressive strength results for the cubes is $f_{c,cube} = 45.7\ MPa$ with a standard deviation of 2.0 MPa, for the cylinders the strength is

$f_c = 38.8\ MPa$ and a standard deviation of 1.8 MPa. Furthermore, the tensile reinforcement was also tested. The measured yield strength is $f_y = 565\ MPa$, ultimate strength $f_u = 683\ MPa$ and modulus of elasticity $E_s = 213\ GPa$. The stress strain diagram is presented in Figure 1

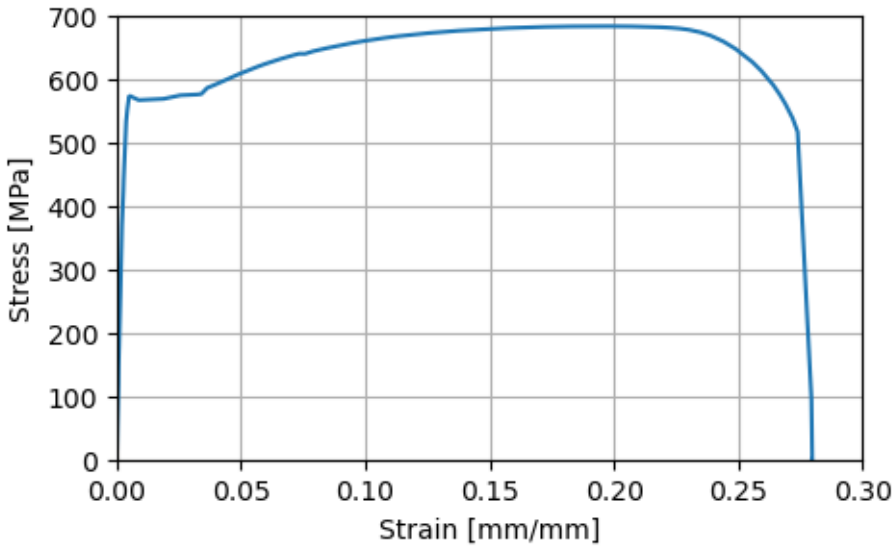

Figure 1. Measured stress-strain diagram for the reinforcement bars

2.2. Panel description

In order to replicate fire exposure conditions for experimental purposes, a innovative high-intensity electric radiant panel is employed. This panel has been custom developed and comprises 21 individual emitters, each measuring 500 mm in length, emitting short-wavelength infrared radiation at high-intensity levels. These emitters collectively cover an area of approximately 900 mm x 500 mm. The emitters are protected by a removable quartz glass panel. When operating at its maximum intensity, the panel can generate an approximately uniform radiative heat flux of $100\ kW/m^2$ over an area measuring 200 mm x 700 mm, positioned at a distance of 100 mm from its protective glass. The measured distribution of the radiative heat flux deviation compared to the central position over that area is shown in Figure 2. The measurements are conducted using a Schmidt-Boelter heat flux gauge positioned at different positions in a grid with with spacing of 10 cm.

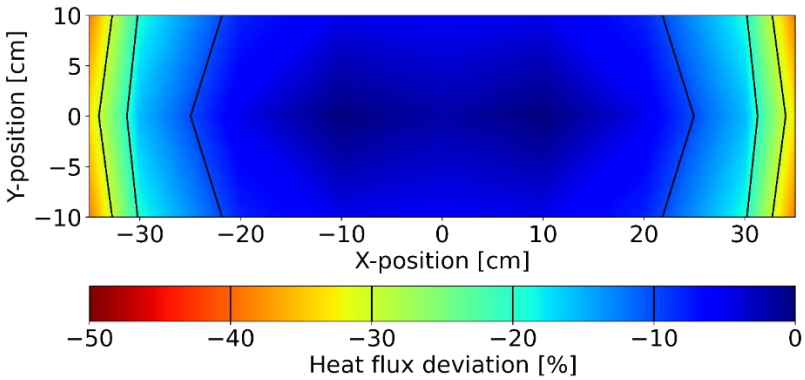

Figure 2 Radiant panel heat flux deviation compared to the central position over the exposed beam area at a 100 mm distance from the panel.

Precise control over the radiation intensity of the panel is achievable through voltage manipulation as an input signal. This control mechanism facilitates the control of the radiative heat flux to which the specimen is exposed based on the previously obtained calibration of the voltage-heat flux relationship [8]. Consequently, it becomes possible to simulate the total heat flux that the specimen would encounter during a fire event at any given point in time, including the decay and cooling phases [9]. This control process is executed using a Python-based in-house program hosted on a PC which allows for dynamic adjustment and monitoring of the radiant heat flux. Further information on the panel characteristics is described in [8].

In the case of a real fire, more precisely a structurally significant flashover compartment fire, the heat is mainly transferred to the structure through convection and radiation [9]. Similarly, the heat transfer to structural elements in accordance with the Eurocode is determined considering convection and radiation relative to a specified temperature-time curve. However, the electric radiant panel is only able to provide radiative heat transfer to the beam specimen. In order to approximate the heat transfer scenario with both convection and radiation, first the total heat flux incoming to the specimen from the chosen temperature-time curve is calculated. This is done numerically using a 1-dimensional finite difference heat transfer model. The surface temperature is calculated based on the convective and radiative heat transfer from the specified temperature-time curve. Finally, using the obtained surface temperature the radiative heat flux needed from the radiation panel to obtain the same total heat flux

on the surface is calculated. It is obtained under the assumption that the convective heat transfer on the exposed surface is negligible. This assumption is derived based on the preliminary tests where it was evident that, due to the small distance between the panel and the exposed beam surface (100 mm), the air in the gap is at temperatures similar to the temperature of the surface and the heated protective glass of the panel. This assumption is further confirmed by comparing the simulated and measured temperatures inside the beams during the tests.

2.3. Setup description

During the first stage of the experiment, the mechanical loading was applied in a reversed four-point bending setup (Figure 3). For safety considerations, the setup was reversed from its standard configuration (upside down) in the first two stages. Specifically, the supports were positioned symmetrically from the midpoint of the beam, with a separation distance of 2100 mm between them. These dimensions were determined based on the constraints imposed by the frame supporting the radiant panel which provides the heating (see Section 2.2). Each support assembly consisted of a steel roller bearing positioned between two steel plates, with one roller being securely welded to the support to prevent horizontal displacement and act as a pin support. The application of loads was carried out at a distance of 100 mm from the edges of the beam, i.e.,750 mm from the support locations.

This reversed setup had several advantages. It allowed the tensioned side of the beam to be positioned on the upper side, facilitating safer and more effective exposure to the radiant panel's heat flux and enabling it to keep the displacements relative to the radiant panel limited without the need for repositioning due to deflections.

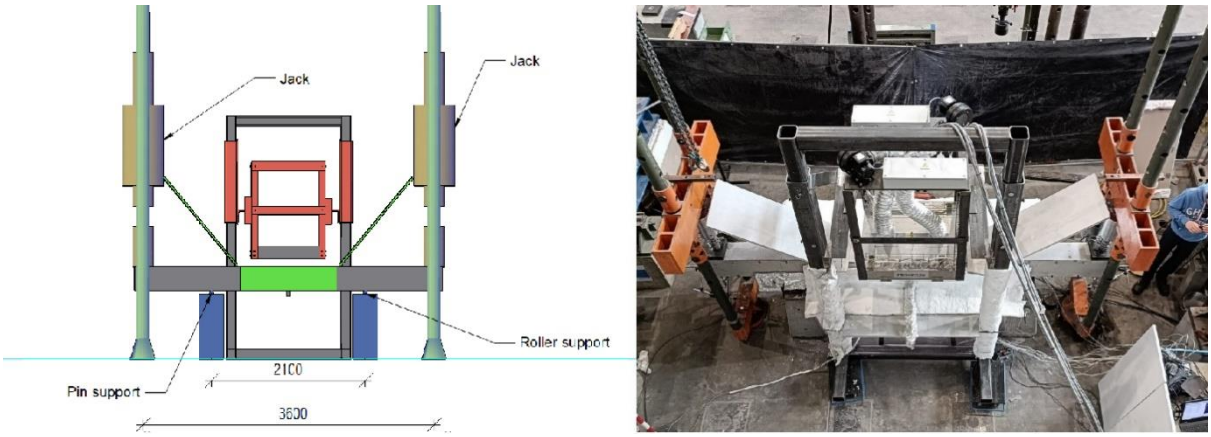

Figure 3. Test setup schematic overview (left); picture of the actual test set-up (right).

Two 200 kN capacity hydraulic jacks with manual pressure control were used for the load application. During the test of beam B1, the pressure control was set up in a way that during the cooling phase, when the deformations started to decrease, the oil level inside the jacks did not decrease and the pressure had to be kept constant by a manual adjustment by opening the valves. This issue was resolved for the tests of beams B2 and B3, by a different configuration of the valves. In this configuration, the oil level would decrease when deformations started to decrease and the pressure was kept constant using the pump.

The middle 700 mm of the beams were exposed to the radiative heat flux from the panel. Considering the reversed 4-point bending setup, this is a zone with a constant bending moment (disregarding the self-weight effect). Insulation boards were used to protect the parts of the top side of the beams that should not experience heating. Furthermore, the sides of the beam were also protected with insulation boards to avoid heat losses at these zones (see Figure 4). This aimed at 1-dimensional heat transfer conditions over the height of the beam with approximately no heat losses on the sides, allowing for an adiabatic surface simplification for modelling purposes. This is confirmed by comparing the temperature results with the numerical simulations as discussed in Section 4.1.

Finally, in the third stage, where the residual capacity was determined, a classical 4-point bending approach was employed. The supports were positioned 100 mm from the edges of the beams, making the total span 3600 mm long. The load was applied with the loading rate of 200 N/s using the same

jacks as in the previous stage but now positioned 1200 mm away from the supports, making the constant moment zone 1200 mm long. As the classical 4-point bending was used, the beam was positioned in a way that the tensioned side of the beam (the one with 3 bars) was on the bottom.. The load was increased until failure. For all beams bending failure was observed, as identified by an accelerating increase in deflection at constant load. For all beams, the deflection at failure was observed to be 4-5 times the deflection at the start of yielding.

Figure 4. Insulation protection on the beams.

2.4. Instrumentation

The load during the tests was applied with two hydraulic jacks with a capacity of 200 kN each. The load was distributed to the concrete beam surface through a steel plate with dimensions of 200 mm x 200 mm x 40 mm. The applied forces were measured by means of two load cells with a capacity of 500 kN, which were placed between the jack and the steel plate.

The vertical displacement was measured using the LVDTs positioned underneath both load application points and at the beam midspan (the side of the beam that was not exposed to the radiant panel). Furthermore, during the heating stage, Digital Image Correlation (DIC) was used to measure displacements in the middle zone of the beams. No significant difference was observed between the

DIC and LVDT measurements of the deflections. A maximum difference of 4 % was observed. Due to the insulation boards on the side of the beam and the high light intensity of the radiant panel itself, only the bottom half of the beam (compressed side) was measured using DIC (see Figure 5). The DIC system employs a pair of Prosilica GT3400 digital cameras, offering a combined resolution of 9 megapixels at 2704x3384@13 Hz on a 1-inch chip. To allow for DIC measurements, the surface of the concrete beam was painted white with black speckles, as shown in Figure 5. The painted speckles have sizes mainly within the range of 0.34 to 0.56 mm, while individual pixels in the images measure approximately 0.10 to 0.13 mm in size. During each test, the image acquisition rate was configured to operate at 1 Hz during the loading phase and 1/15 Hz during the heating and cooling phases. Subsequent image processing was conducted using the VIC-3D software developed by Correlated Solutions [10]. Regarding the quality of displacement measurements estimated through the DIC equipment, the observed noise levels differed for in-plane and out-of-plane displacements. For in-plane displacements, the noise level was quantified as approximately 0.004 mm, determined as the average between the highest and lowest displacement values. Meanwhile, for out-of-plane displacements, the noise level was estimated to be approximately 0.007 mm.

Figure 5. The compressed side of the beams monitored using the Digital Image Correlation (DIC).

In order to monitor the temperature distribution inside the beam, 18 type-K thermocouples (diameter 0.4 mm) were cast inside each beam. The thermocouples were positioned in three different positions along the length of the beams: the middle sections and two sections 300 mm on each side from the midpoint (refer to Figure 6). At each of these three positions, 6 thermocouples were positioned at

different depths from the heat-exposed surface: 12 mm (in the middle of the shear reinforcement on the outer side), 20 mm (connection of the main and shear reinforcement in the tension zone), 50 mm, 100 mm, 150 mm and 278 mm (Figure 7). Their position was secured using 2 mm thick steel wire connected to the reinforcement cage of the beam, fixing the thermocouples during the casting process.

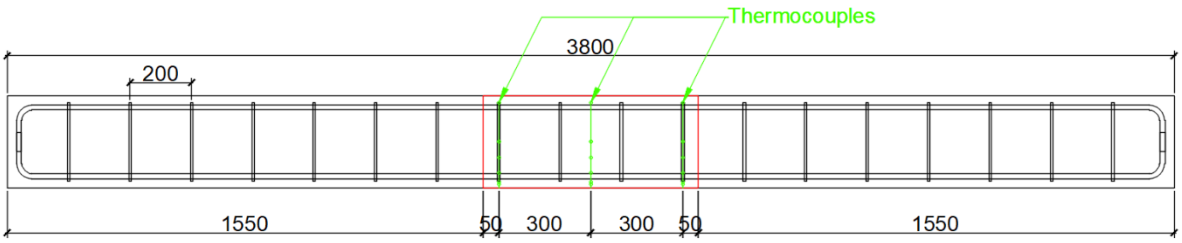

Figure 6. Position of the thermocouples cast inside the beams in the longitudinal direction. (red box represents the heated area)

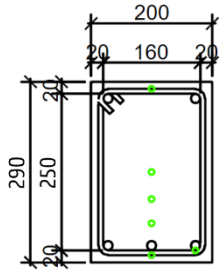

Figure 7. Position of the in-depth thermocouples cast inside the beams in the cross-section.

3. Experimental results

3.1. Loading and unloading phase

The first stage of the testing procedure, which was conducted on all beams (B1, B2, B3 and BR), consisted of the loading and unloading of the beams. This stage was conducted for the needs of the larger testing campaign, more precisely to obtain reference measurements on the beams that already experienced damage due to the expected serviceability load, but without heating exposure.

The beams were loaded with a loading rate of approximately 200 N/s up to a load of 55 kN on each side. At this load value, the bending moment reaches a value of 41.25 kNm in the central zone of the beam. This amounts to 67% of the design moment capacity of the beam.

Figure 8 shows the force-deflection diagram for all four tested beams. It can be noted that, as expected, the behaviour of all beams is similar. The slope of the curves changes at approximately 13 kNm (17.3 kN force) for all beams. This is in line with the expected cracking moment of 12.7 kNm (17 kN). After the unloading, the formation of the cracks in the tension zone was noticed. The cracks were on average approximately 150 mm deep occurring approximately every 100 mm in the midspan zone with the constant moment.

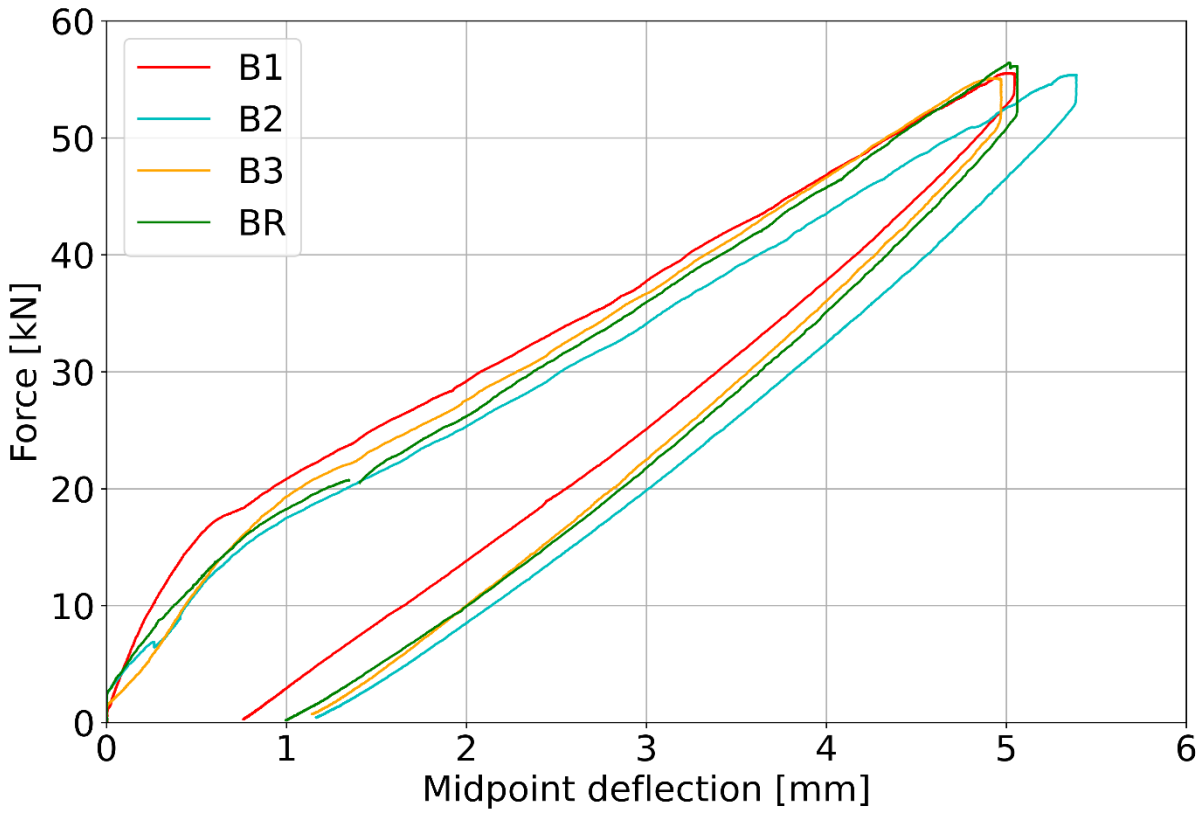

Figure 8 Force-displacement diagram during the cracking phase of testing

3.2. Fire exposure phase

In the fire exposure phase, natural fire exposure was simulated using the Eurocode Parametric Fire Curve (EPFC) . In accordance with the capabilities of the radiant panel, EPFC with $\Gamma = 0.45$ (factor

defining the temperature increase during the heating phase) and a heating phase duration of 1 hour was chosen. The maximum gas temperature for this temperature-time curve is 826 °C and the total fire exposure lasts 233 min. The heat flux applied with the radiant panel is calculated in order to provide the same total heat flux to the surface of the beam as the EPFC. The radiative heat flux peaks at $85.75\ kW/m^2$ and is stopped at 196 min when the total heat flux becomes negative (the surface temperature is higher than the gas temperature). The desired temperature-time curve and heat flux are shown in Figure 9. The beams B1, B2 and B3 were exposed to the heating 125, 140 and 182 days after casting respectively.

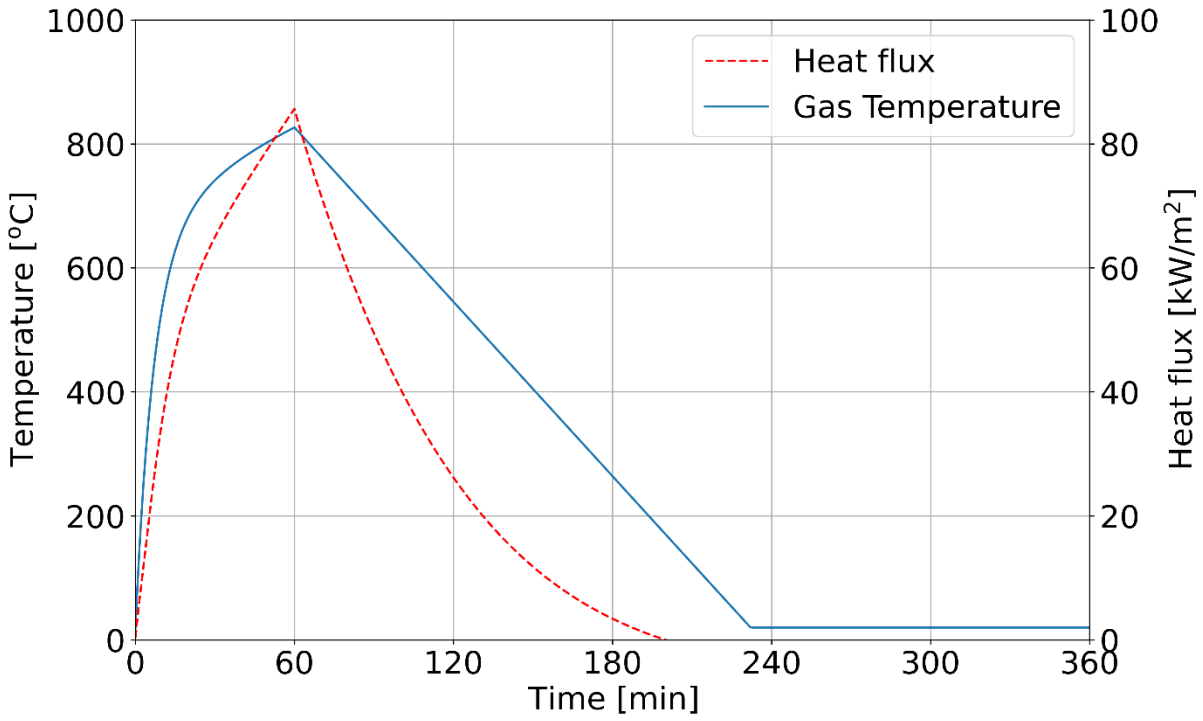

Figure 9 Eurocode Parametric Fire Curve temperature-time curve and equivalent radiant heat flux from the panel.

During the test, the heat flux at the surface of the beam was measured with a water-cooled Schmidt-Boelter heat flux meter. The heat flux meter was positioned next to the beam, levelled with the exposed surface of the beam in the middle of the exposed zone. The heat flux meter was connected to the beam in a way to stay in level with it even when the beam starts deforming. Figure 10 presents the results of the measurements for all three beams. It can be noted that the measured heat flux for all three tests was almost identical, demonstrating that all beams were exposed to the same heat flux. However, it is

264 also clear that the measured heat flux was higher than the intended one. This difference can be mostly
265 attributed to the effect of convection from the hot air around the heat flux meter. This convective effect
266 was quantified, assuming that the hot air temperature around the heat flux meter is equal to the
267 intended surface temperature of concrete using an approximate convective heat transfer coefficient of
268 20 W/(m^{2}K). The comparison between the measured and this adjusted heat flux suggests that the
269 exposed surface of the beam did receive the intended radiative heat flux.

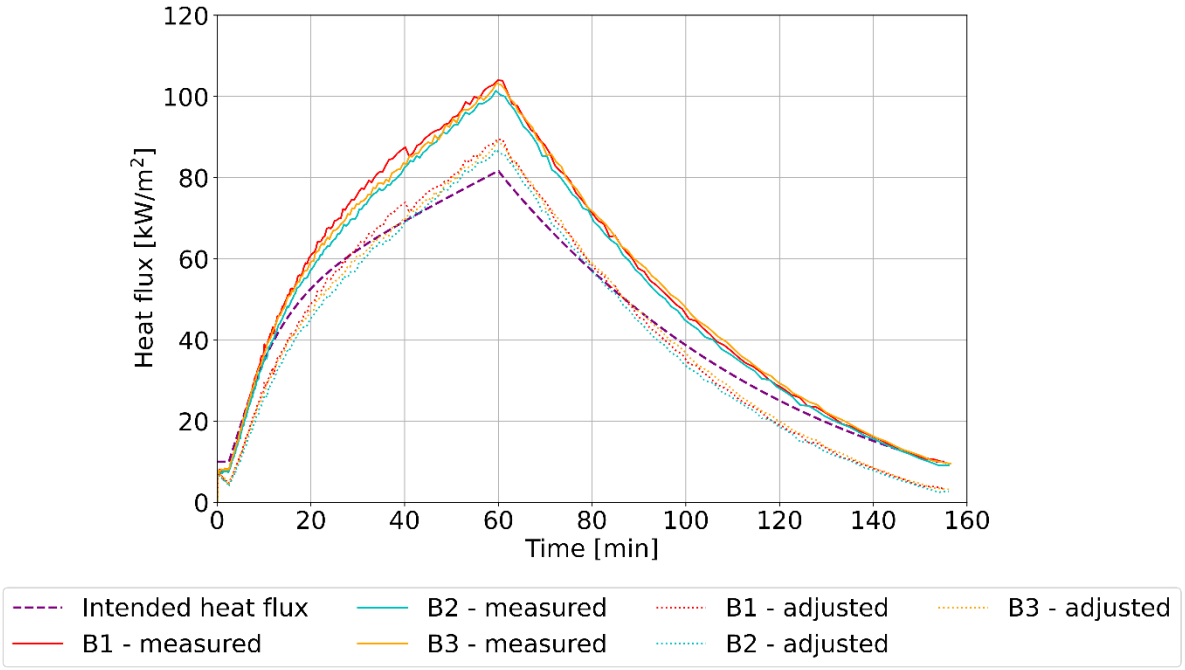

270

271 *Figure 10 Measured and intended radiative heat flux during the tests. After 155 min, the panel was shut down and the beam*
272 *was allowed to cool naturally.*

273 As mentioned in Section 2.4 the temperatures inside the beams were measured at 3 longitudinal
274 positions along the beam length, using 6 thermocouples cast inside the beam at each location, as
275 illustrated in Figure 6 and Figure 7. Figure 11 shows the measured temperature at depths of 20 mm, 50
276 mm and 150 mm from the exposed surface for each of the three measurement locations for beam B2.
277 Figure 10 demonstrates that the heating was symmetrical as the temperatures at the left and right
278 sides of the heated zone are almost identical. However, the temperatures in the middle are higher. This
279 is a consequence of the non-uniformity of the radiative heat flux (Figure 2) and the higher influence of

the heat conduction to the unheated parts of the beam. Similar results are observed in all beams and at all thermocouple depths.

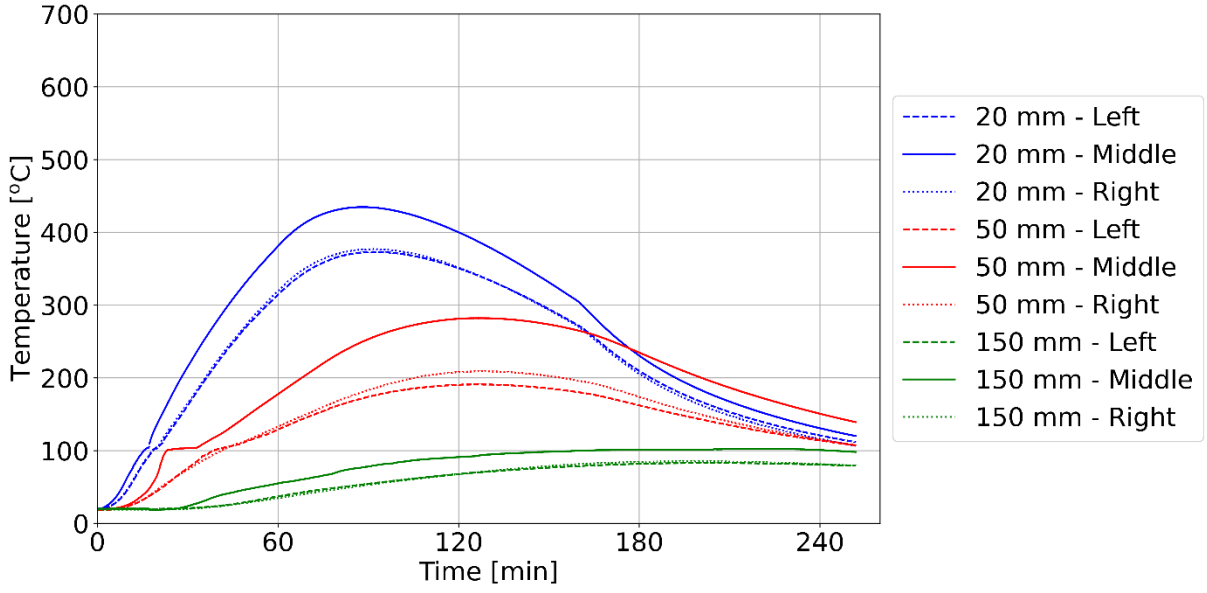

Figure 11 Measured temperatures at different depths and positions during the test of beam B2.

Figure 12 presents the temperatures in the middle section of all three beams at different depths. It can be observed that the temperatures for all three beams do not differ significantly from each other. The largest differences are closest to the exposed surface at a depth of 12 mm. The thermal gradient at this position is the steepest and small variations of the thermocouple position can have a significant effect on the measured temperature. However, even at this position, the temperature difference does not exceed 10%. In the case of the other depths, the difference is almost negligible.

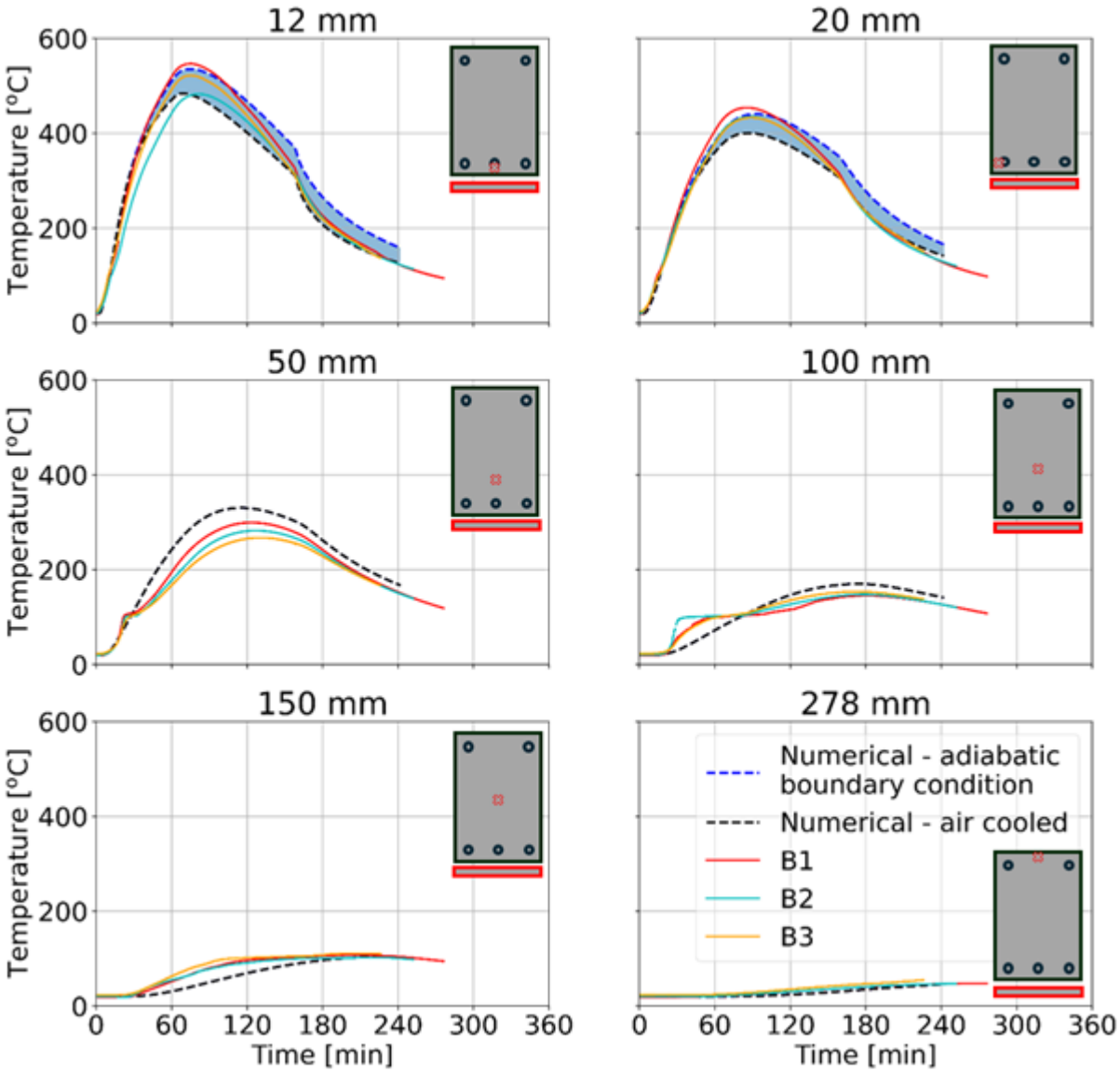

290

291 *Figure 12. Temperatures at the midspan section measured during all three tests at different depths compared to the numerical*
292 *results. A distinction is made between (i) adiabatic and (ii) air-cooled numerical results related to the modelling of the*
293 *boundary condition for the side of the beam.*

294 For all depths, especially the larger ones, a plateau at 100 °C is evident. This plateau is reached because
295 of the moisture present inside the beam [11] and is caused by water evaporation and moisture transfer
296 inside the beam. Additionally, it should be noted that after approximately 30 minutes in each test,
297 water droplets on the unexposed sides of the beams were observed.

298 After, 155 minutes, when the radiative heat flux was lower than 10% of the maximum one, the panel
299 was shut down. This moment can also be observed in Figure 12. At that point, the thermal boundary

condition changes, as there is no more radiative heat flux at the surface and the convective cooling commences. When looking at the temperatures close to the surface (at depths of 12 and 20 mm) it is evident that the cooling regime changes. At higher depths this effect is negligible.

In Figure 13 the temperatures in the middle of the beams at different points in time are presented, considering linear interpolation between the measured temperatures at different depths in order to visualize the temperature gradient. It is evident that the variation of the thermal gradient inside of the beam between the tests is quite small, demonstrating again a high level of repeatability between the tests. The figure also shows that even after the heating phase ends (60 min) the temperature still increases deeper into the beam, as expected.

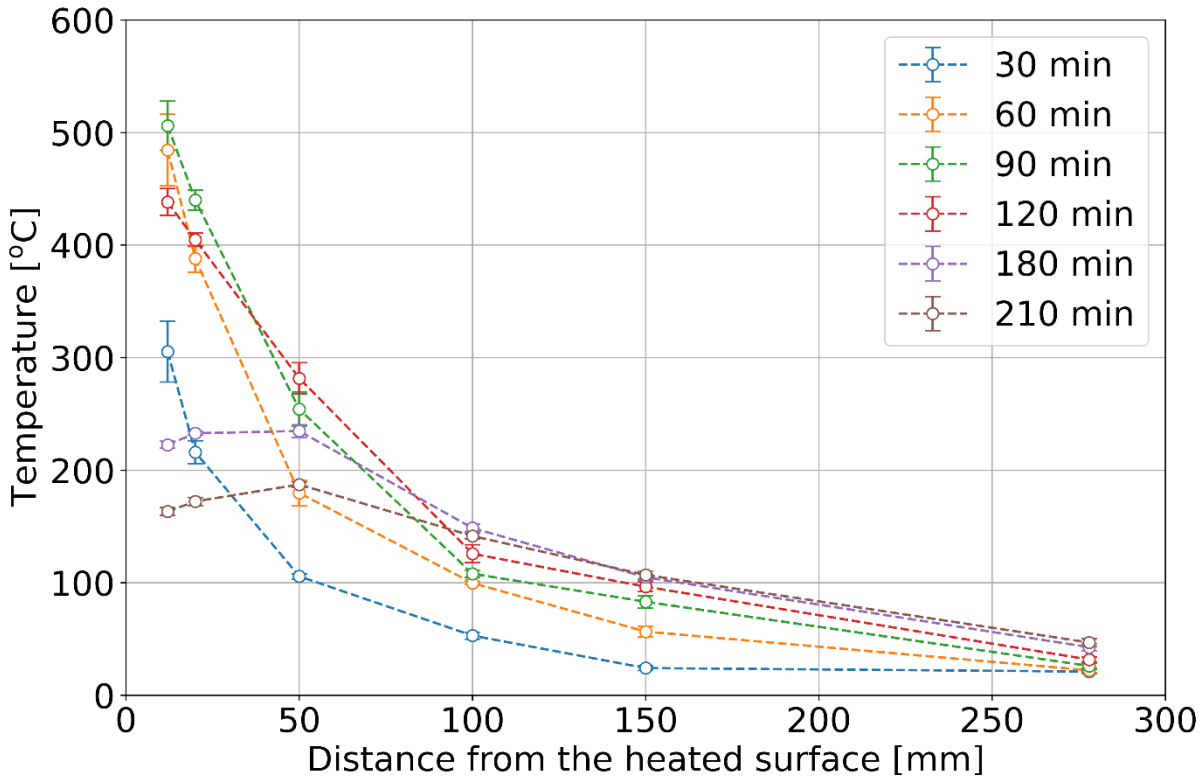

Figure 13. Thermal gradient inside of the beams at different points in time (error bar represents the standard deviation between the beams).

The midspan deflection for all three tested beams is presented in Figure 15. The deflections are presented in the form of deflection relative to the deflection at the start of the heating regime (i.e., 0 mm refers to the deflection under the application of the serviceability load prior to the heating regime).

During the first 60 minutes, while the applied heat flux was increasing, an almost linear increase in the deflections can be observed. The deflections continue to increase at a slower rate until approximately 95 minutes when they reach their maximum for all three beams. From that point, the deflections remain approximately constant for 15 min before slowly reducing. Similar to the temperatures, when the panel is turned off at 155 min the rate of the decrease of deflections changes.

For beam B1, as mentioned in Section 2.4, the hydraulic jacks had to be controlled through a manual release of pressure during the cooling phase, more precisely when deformation started to decrease. This could be done only through abrupt actions and is the reason for the step-wise behaviour of the deflections in Figure 13. For beams B2 and B3, this was resolved by a change in the setup of the pressure control mechanism. The forces applied to the beams are presented in Figure 14.

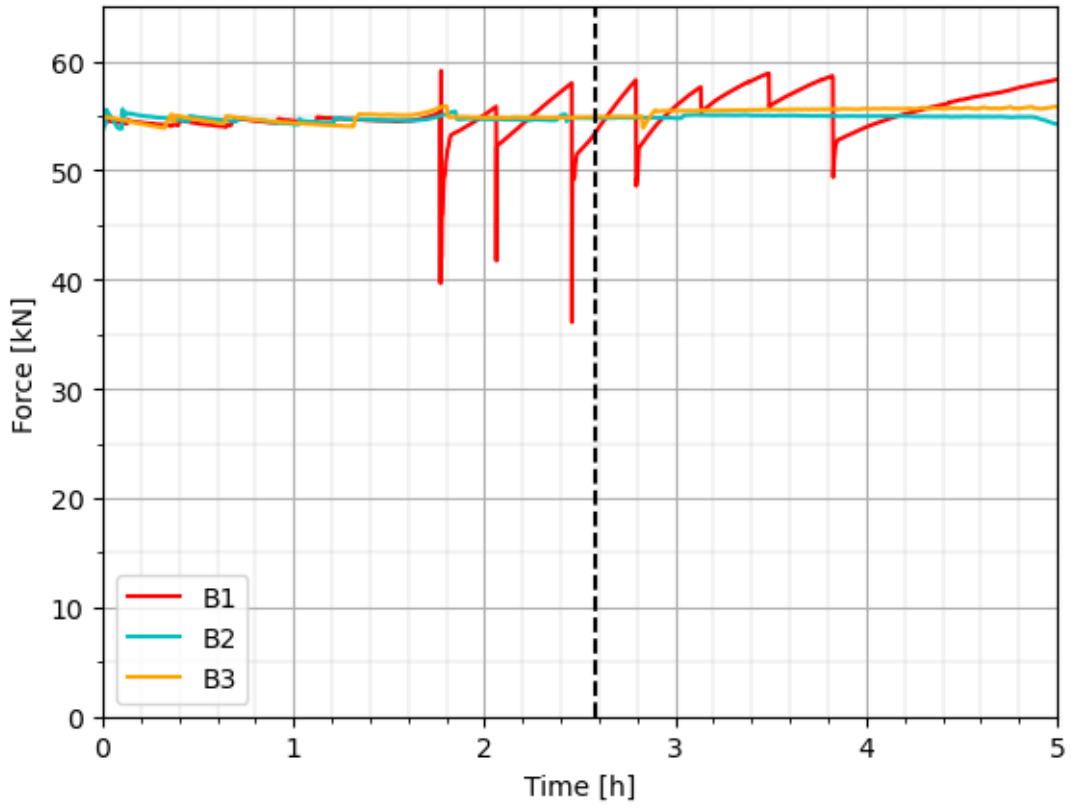

Figure 14. Applied forces during the tests. The dashed line represents the moment when the radiant panel was shut down.

The average displacements under the load application points are shown in Figure 16. The deflections are presented in the form of deflection relative to the deflection at the start of the heating regime (i.e.,

0 mm refers to the deflection under the application of the serviceability load prior to the heating regime). Similar to the midspan deflection, the deformations under the loading points are consistent between the three tested beams. Furthermore, the same general behaviour can be observed.

Finally, using the DIC, the curvature in the zone with the uniform moment was obtained. As the DIC measurements enabled to monitor the movement for every point in this zone for the compressed half of the beam, the curvature could be calculated using two different approaches. Firstly, the average vertical displacement was calculated for every 1 cm wide vertical strip of the monitored area. These deformations show an almost perfect match to the parabolic curve. The curvature was obtained as the second derivative of this curve. The second approach consisted of obtaining the total strain diagram in the function of the height, averaged out on the whole monitored area. These total strain diagrams showed a linear trend, validating the assumption in the Euler-Bernoulli beam theory of plain sections remaining plain, even at elevated temperatures. The curvature is calculated as the slope of this total strain diagram. These two methods produced almost identical results with less than 2% difference in the values. The change of the curvature in the heated zone is shown in Figure 17 (using the first method) and similar trends as for the midspan and load point deformations can be observed.

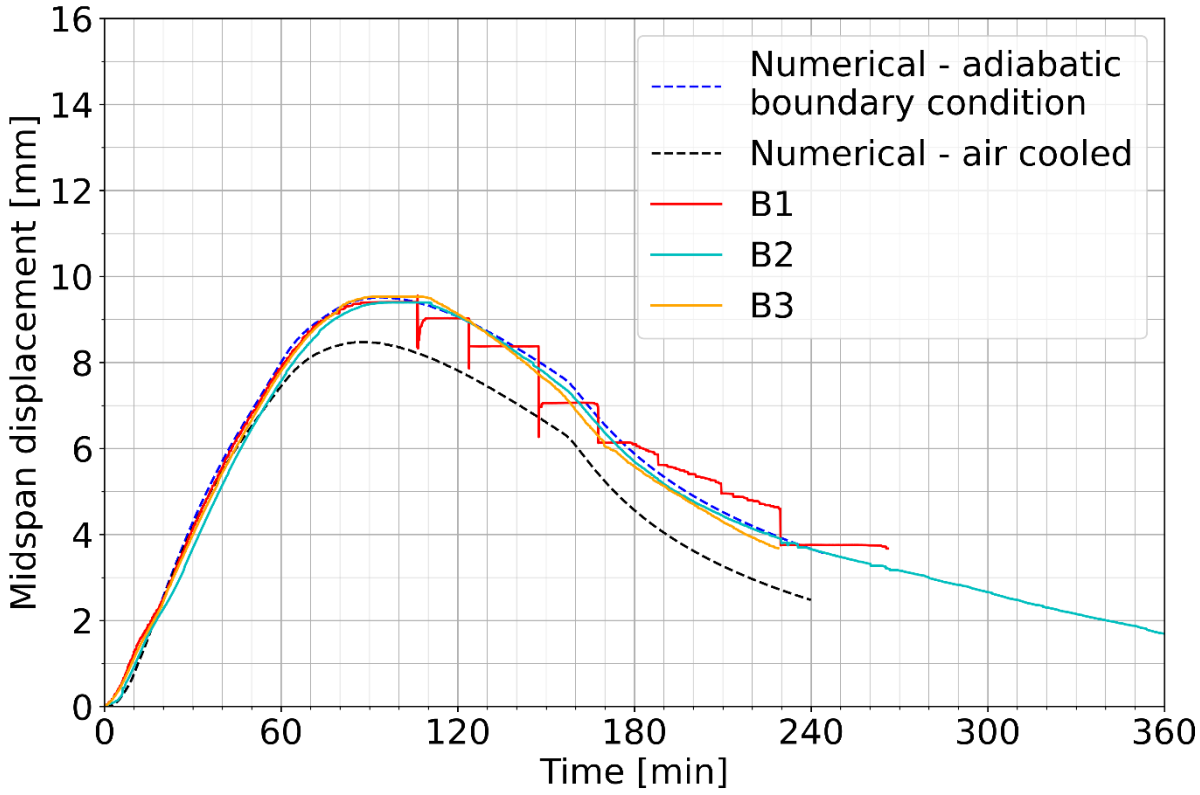

344

345 *Figure 15. Midspan displacement during the tests compared to the results of numerical simulations*

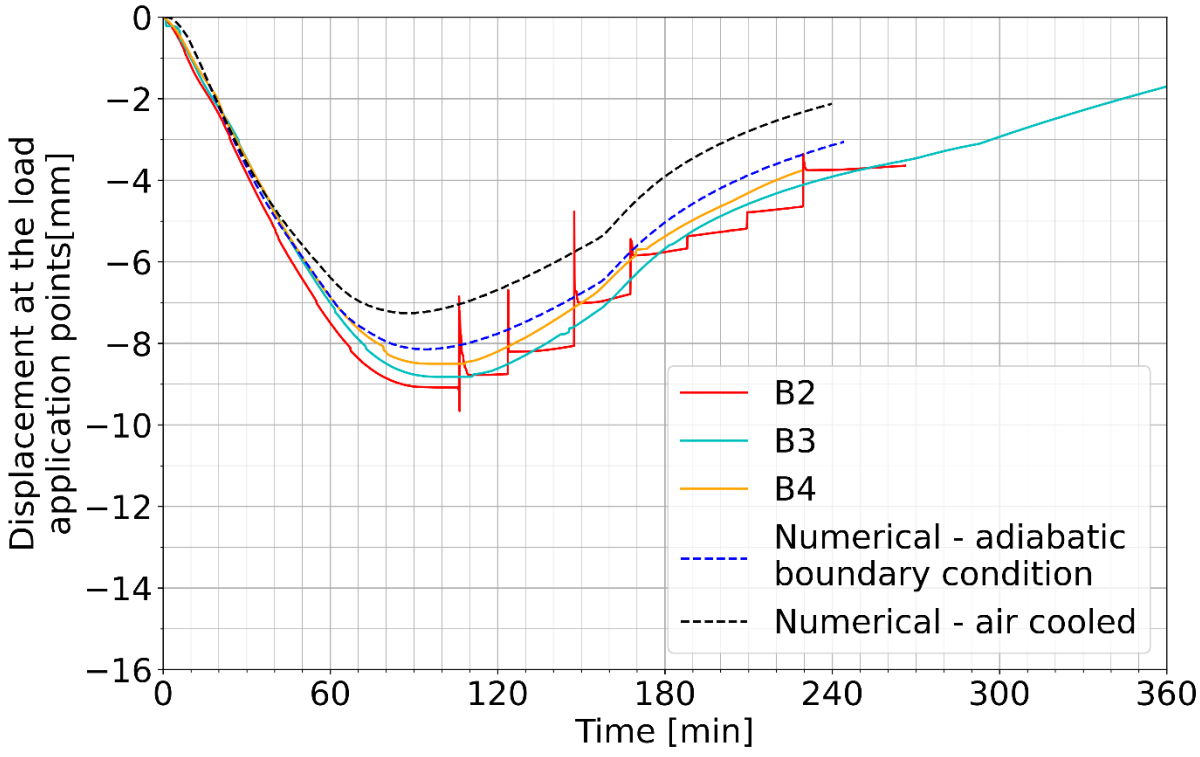

346

347 *Figure 16 The average displacement at the load application points during the tests compared to the results of numerical*

348 *simulations.*

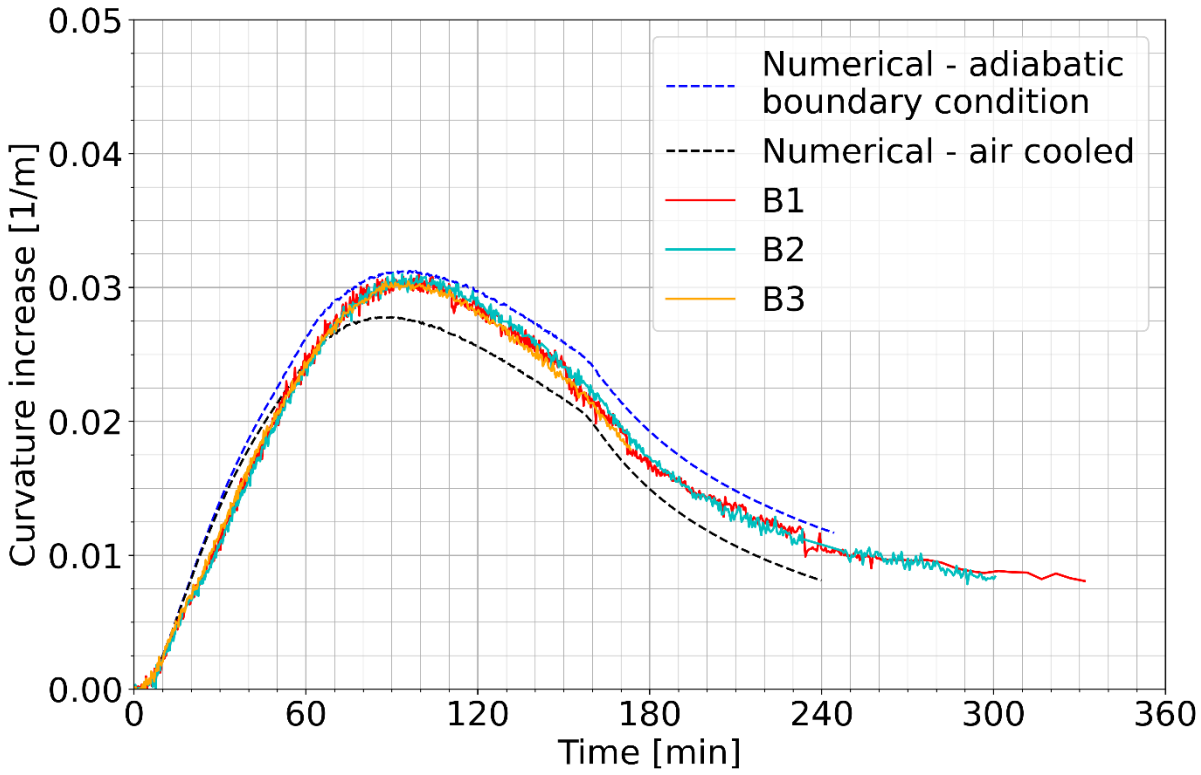

Figure 17. Curvature increase during the tests compared to the results of numerical simulations.

3.3. Residual capacity tests

This stage was conducted on both the beams exposed to elevated temperature (B1-B3) and the reference beam BR. Its purpose was to determine the residual bending capacity of beams B1-B3 and compare it to the residual bending capacity of the non-fire exposed beam BR. For that purpose, a standard 4-point bending setup was employed. These tests were conducted 160, 147 and 107 days after the heat exposure for the beams B1, B2 and B3 respectively. Figure 18 shows the force–midspan deflection diagram for all the beams. From the figure, it is evident that the heating exposure did not have a large effect on the bending stiffness of the beams, as the initial slope of the curve for the beam BR is similar to the slope of heat-exposed beams. However, the overall shape of the curves differs. For beams B1-B3 a linear behaviour is observable until a deflection of about 25 mm is reached, which is the onset of a clear plateau in the diagram.

In the case of the bending moment capacity, there appears to be a significant difference between them. The values of the bending moment capacity are shown in Table 2. The coefficient of variation of the

values for beams B1-B3 is 0.2%, while the value for BR is around 8% higher demonstrating a clear reduction in the ultimate bending capacity due to the heat exposure.

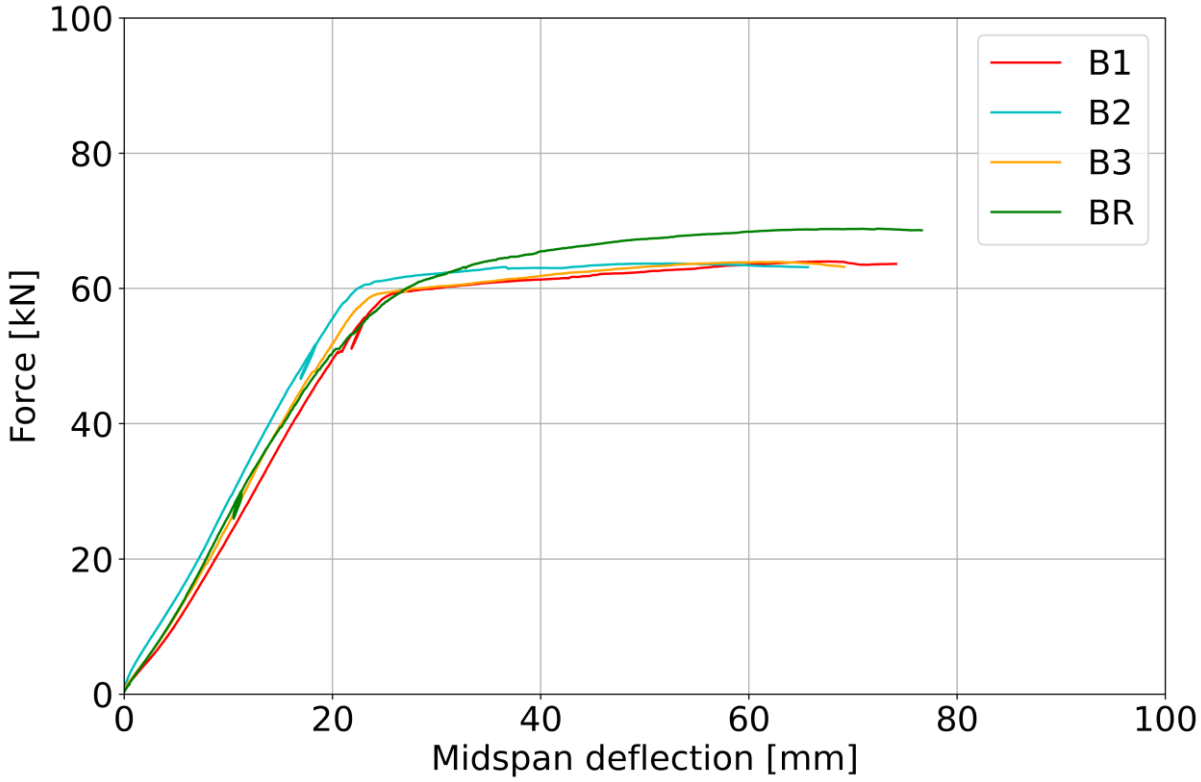

Figure 18. The force–midpoint deflection diagram for beams B1-B3 and BR during the residual capacity tests.

Table 2. Ultimate bending moment capacity of the beams B1-B3 and BR

Beam	B1	B2	B3	BR
Bending capacity - M_R [kNm]	76.8	76.4	76.7	82.6

4. Numerical modeling

A finite element model of the tested beams was developed in the finite element software SAFIR [12], which specializes in the modelling of the structural behaviour of structures exposed to fire. The analysis

consists of two parts. First, the heat transfer analysis is conducted in order to obtain the temperature-time history of the structure and afterwards, that data is used to conduct the structural analysis.

4.1. Heat transfer

The heat transfer analysis was conducted considering a 2-dimensional model focusing on the heat transfer inside the cross-section. The cross-section was divided into 1320 rectangular elements with size varying from 4 to 8 mm. The concrete was modelled as defined in EN 1992-1-2 (3.3) [7] (SILCON_EN). The default values were used: concrete density $\rho_{con} = 2400 \frac{kg}{m^3}$, water content $w = 46\ kg/m^3$ and thermal conductivity as average of upper and lower limit. The steel reinforcement was modelled according to thermal properties defined in EN 1993-1-2 . The radiation and convection boundary conidtions are considered for the tensioned edge of the cross-section using a single temperature-time curve. As stated in Section 3.2 (Figure 9), the temperature-time curve considered was an EPFC with $\Gamma = 0.45$ and a heating phase duration of 1h. As the panel was shut down after 155 min, the cooling branch of the EPFC was modified as follows: the EPFC cooling branch was followed up to 155 min, after which the temperature-time curve was considered to instantaneously drop to 20 °C. The radiative heat transfer considered an absorptivity/emissivity of the concrete surface of 0.7 and convection was calculated considering a convection coefficient of 35 W/(m^{2}K), both in accordance with the Eurocode provisions . On the compressed side, convective and radiative heat losses are considered relative to a constant reference temperature of 20 °C. This was done considering an emissivity of 0.7 and a convection coefficient of 4 W/(m^{2}K) .

As mentioned before, the sides of the beams were protected from the incoming radiation using insulation boards. However, to enable additional instrumentation, an air gap of approximately 15 mm between the board and the beam was left. As the air in the gap would work as an insulation, the actual boundary condition on the sides was close to the perfect insulation and it was modelled in that way (i.e., adiabatic boundary condition).

In Figure 12 the results of the heat transfer analysis are shown together with the measurements of the thermocouples during the test. Overall it can be concluded that the simulation results correspond well with the measured values at all depths. At larger depths, we can see that the numerical simulation is not able to properly capture the plateau at 100 °C. This is a commonly known shortcoming of the heat transfer calculations of concrete members where the moisture transfer is neglected, see e.g., [13]. Even though the energy of evaporation is accounted for in the specific heat of concrete definition according to EN 1992-1-2 [7], it assumes that moisture is uniformly distributed over the entire cross-section for the full duration of the heat exposure. However, in reality, due to the thermal effects, the moisture content migrates to the cooler parts. For this reason, we can observe a faster rise to 100 °C in the measured data at higher depths, as more energy is brought with the moisture transfer, which condenses in the cooler zones of the concrete, increasing the moisture concentration there [14]. Because of this increased moisture concentration, the energy needed for evaporation is higher which in turn causes a longer plateau.

4.2. Structural analysis

In the structural analysis, the beam is modelled as a 2-dimensional fibre model (the determination of forces and stiffness in the section is based on the temperatures in each element used in the thermal analysis which form a fibre in the beam element) with a length of a 3.6 m (distance between the load application points), consisting of 72 elements of 0.05 m length. For the middle 14 elements, the temperature-time history as obtained through the previously discussed heat transfer calculations is used, while the other elements remain at a temperature of 20 °C throughout the whole simulation. The mechanical boundary conditions are modelled as they were implemented in the tests (roller and pin support) and the load is introduced as two vertical forces with a constant value of 55 kN positioned at the ends of the beam.

The concrete model used is a direct implementation of the explicit transient creep model introduced by [15] (SILCON_ETC). Input material properties needed for this model were based on the measured

values: concrete compressive and tensile strength $f_c = 45.7\ MPa$ and $f_t = 2.9\ MPa$. During the cooling process, the mechanical properties of strength and strain at peak stress are not recoverable. A further reduction of 10% in the concrete's compressive strength, relative to the value at the maximum temperature reached, is accounted for during cooling, as outlined in [16]. The reinforcement was modelled using the model which is defined in EN 1992-1-2 (3.3) [7] (STEELEC2EN), similarly, the measured yield strength of $f_y = 565\ MPa$ is used together with the modulus of elasticity $E_s = 213\ GPa$ as needed input values.

A comparison of the calculated midspan deformation with the ones measured during the tests is presented in Figure 15. Overall, the model is able to predict the behaviour observed in the tests rather accurately. This is also highlighted by the fact that the simulation results do not differ from the measured values more than the three identical beams tested in a fundamentally identical way differ from each other.

The agreement between the numerical simulation and measured results is much higher in the case where the boundary condition on the side edges is modelled as adiabatic. This observation is in line with the previous observation that the agreement between temperatures is also higher in this case, especially in the heating phase.

Similar agreements can also be seen in Figure 16 which represents the additional deflection during the heating and cooling of the beam at the position of the load points (i.e., the beam extremities). When the curvature behaviour is analyzed in Figure 17, a very close agreement between the tests and model is obtained

5. Discussion

The heat transfer was modelled with perfect insulation. However, due to the existence of the air gap during the tests, the real heat loss condition is quite difficult to model precisely. In order to assess this, the boundary condition on the side edges was modelled in an additional way. It was modelled as the

side edges are exposed to the ambient air, by considering the same cooling conditions as for the compressed edge. This is illustrated in Figure 19.

The test results show better agreement with the case where the side edges are modelled as adiabatic, especially in the first 120 min, afterwards the shift to the case with the ambient air on the sides is observed. This can be explained by the air temperature in the gap during the test. It can be assumed that during the heating phase of the test, the air temperature also rose causing any heat transfer on the side negligible. After the temperatures of the beam started dropping the air in the gap, due to its thermal properties, started to cool down faster and caused faster cooling of the sides of the beams. The effect of the different boundary conditions on the side edges is almost negligible at larger depths.

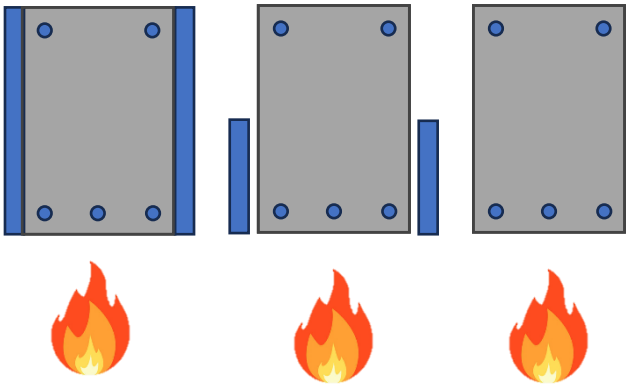

Figure 19. Different cases for modelling boundary conditions on the side edges of the concrete beams: full insulation (left), real scenario during the tests (middle; this case is not directly modelled) and ambient air contact (right).

When considering the residual bending capacity, it can be noted that the three beams exposed to elevated temperatures showed great uniformity in the obtained bending capacity with a 0.2% coefficient of variation. The three beams show an 8% lower capacity than the reference beam BR. The source of this difference can be traced to the reduction of the yield strength of the reinforcing steel as the temperature in the compressed half of the beams B1 to B3 never reached more than 100 °C. Even though it is commonly agreed that the reinforcement steel retains 100% of its yield strength after cooling when its temperature does not exceed 500 °C [17], as was the case for beams B1 to B3, experimental data from [18], [19], [20], [21], shows that a reduction offor this temperature range, of

order of magnitude of 0-7% has been recorded. Considering that, an 8% reduction in ultimate bending capacity due to a decrease in reinforcement yield strength is a reasonable hypothesis, however a further investigation in the future is needed to confirm this.

6. Conclusions

An innovative electric radiant panel has been used in order to simulate a natural fire exposure of concrete beams. The tests described herein are conducted to produce three identically fire-damaged beams, which are tested to assess their post-fire condition. Despite minor limitations related to the heated area's size and the maximum heat flux, it showed great performance in the sense of control and repeatability. The preliminary phase, involving mechanical loading and unloading tests, yielded crucial baseline data, with the observed crack formations aligning with theoretical expectations.

Temperature measurements within the beams demonstrated an almost uniform thermal field between all the beams, with minor discrepancies easily attributed to precise thermocouple placement. Comparisons with numerical simulations of the temperature field confirmed the efficacy of the experimental setup in replicating natural fire conditions, notably the EPFC temperature-time curve, despite the panel producing only a radiative heat flux.

The structural response of the beams during the heating phase exhibited distinct phases. Initially, there was a linear increase in deflection, followed by a slower rate of deflection increase. The beams reached their maximum deflection, after which they exhibited a plateau before slowly reducing deflections during the cooling phase. These observations align with expected behaviour under fire exposure conditions. A similar high level of repeatability and consistency is observed to the one observed with temperatures. Deformations for all three beams are similar to each other, showing the same trends both in the heating and cooling.

In regards to the residual bending capacity of the beams, the results showed large uniformity across the beams exposed to elevated temperature. The beam not exposed to high temperatures showed a

slightly higher bending capacity, effectively demonstrating that some amount of damage occurred due to temperature exposure.

The FEM analysis proves to be a precise tool for simulating the behaviour of concrete members subjected to fire conditions. Prior modelling with readily available state-of-the-art simulation tools align very well with the observed test results. Thus, the test results can be considered as a validation of said the applied simulation tools.Modelling using SAFIR has proven to be able to assess the temperature field in the beams with reasonable accuracy. The inability to model the moisture transfer is a deficiency, especially when higher depths are considered, however, they do not have a large effect on the global behaviour of the member.

The model accurately predicted the structural response during the heat exposure. The differences between the numerical results and the tests' results are on the same scale as the differences between the tests themselves. A high potential for assessing concrete member behaviour in fire scenarios is demonstrated based on these results.

In summary, this research contributes to the field of fire engineering by demonstrating a reliable and innovative testing approach for simulating fire-induced damage on concrete members. The use of a innovative electric radiative panel, combined with accurate natural fire exposure conditions, offers a promising avenue for evaluating the post-fire behaviour of concrete structures. The repeatability and consistency of results across multiple tests enhance the credibility of the findings. Furthermore, the applied numerical simulations' accuracy reinforces their potential utility in assessing and predicting concrete structures' behaviour under fire conditions.

Acknowledgements

The authors wish to thank the Research Foundation of Flanders (FWO) for the financial support on the research project (Grant number 3G010220) "Vibration-based post-fire assessment of concrete structures using Bayesian updating techniques". Andrea Lucherini is funded by the FRISSBE project

within the European Union's Horizon 2020 research and innovation program (GA 952395) and Florian Put is funded by Research Foundation of Flanders (FWO) within the scope of the research project (Grant number 1137123N) "Characterization of the thermal exposure and material properties of concrete during the fire decay phase for performance-based structural fire engineering". The authors further thank dr. Ramin Yarmohammadian for the useful comments on the manuscript.

References

[1] J. Beitel and N. Iwankiw, "Historical Survey of Multi-Story Building Collapses Due to Fire," *Fire Prot. Eng.*, vol. 27, 2005.

[2] fib, Fédération International du Béton, *fib Bulletin 108. Performance-based fire design of concrete structures*. 2023. doi: 10.35789/fib.BULL.0108.

[3] B. Jovanović, R. Caspeele, G. Lombaert, E. Reynders, and R. Van Coile, "State-of-the-art review on the post-fire assessment of concrete," *Struct. Concr.*, 2023.

[4] fib Fédération International du Béton, *Fib bulletin 38: fire design of concrete structures—materials, structures and modelling, state-of-the art report*, vol. 53. 2007.

[5] T. Gernay *et al.*, "Experimental investigation of structural failure during the cooling phase of a fire: Concrete columns," *Fire Saf. J.*, vol. 134, p. 103691, Dec. 2022, doi: 10.1016/j.firesaf.2022.103691.

[6] C. Maluk, L. Bisby, M. Krajcovic, and J. L. Torero, "A Heat-Transfer Rate Inducing System (H-TRIS) Test Method," *Fire Saf. J.*, vol. 105, pp. 307–319, Apr. 2019, doi: 10.1016/j.firesaf.2016.05.001.

[7] CEN, "EN 1992-1-2:2004: Eurocode 2: Design of concrete structures - Part 1-2: General rules. Structural fire design." European Standard, 2004.

[8] F. Put, B. Jovanović, E. Symoens, A. Lucherini, B. Merci, and R. Van Coile, "High-Intensity Fast-Response Electric radiant Panel (HIFREP) for increased accuracy on thermal boundary conditions during fire testing," *4th Eur. Symp. Fire Saf. Sci. – ESFSS 2024*, in press.

[9] A. Lucherini and J. L. Torero, "Defining the fire decay and the cooling phase of post-flashover compartment fires," *Fire Saf. J.*, vol. 141, p. 103965, Dec. 2023, doi: 10.1016/j.firesaf.2023.103965.

[10] Correlated Solutions, *Vic-3D*. (2010). Correlated Solutions Inc. [Online]. Available: www.correlatedsolutions.com/supportcontent/VIC-3D-8-Manual.pdf

[11] H. Lakhani, P. Kamath, P. Bhargava, U. Sharma, and G. Reddy, "Thermal Analysis of Reinforced Concrete Structural Elements," *J. Struct. Fire Eng.*, vol. 4, no. 4, pp. 227–244, Jan. 2013, doi: 10.1260/2040-2317.4.4.227.

[12] J.-M. Franssen and T. Gernay, "Modeling structures in fire with SAFIR®: theoretical background and capabilities," *J. Struct. Fire Eng.*, vol. 8, no. 3, pp. 300–323, Jan. 2017, doi: 10.1108/JSFE-07-2016-0010.

[13] J. V. Aguado, V. Albero, A. Espinos, A. Hospitaler, and M. L. Romero, "A 3D finite element model for predicting the fire behavior of hollow-core slabs," *Eng. Struct.*, vol. 108, pp. 12–27, 2016.

[14] T. Z. Harmathy, "Effect of Moisture on the Fire Endurance of Building Elements," in *Moisture in Materials in Relation to Fire Tests*, A. F. Robertson, Ed., 100 Barr Harbor Drive, PO Box C700, West Conshohocken, PA 19428-2959: ASTM International, 1965, pp. 74-74–22. doi: 10.1520/STP48429S.

[15] T. Gernay and J. M. Franssen, "A formulation of the Eurocode 2 concrete model at elevated temperature that includes an explicit term for transient creep," *Fire Saf. J.*, vol. 51, pp. 1–9, 2012, doi: 10.1016/j.firesaf.2012.02.001.

[16] CEN, "EN 1994-1-2:2005 Eurocode 4: Design of composite steel and concrete structures - Part 1-2 General rules - Structural fire design," *European Standard*. European Standard, 2005.

[17] V. K. R. Kodur and A. Agrawal, "An approach for evaluating residual capacity of reinforced concrete beams exposed to fire," *Eng. Struct.*, vol. 110, pp. 293–306, 2016, doi: 10.1016/j.engstruct.2015.11.047.

[18] I. C. Neves, J. P. C. Rodrigues, and A. de P. Loureiro, "Mechanical Properties of Reinforcing and Prestressing Steels after Heating," *J. Mater. Civ. Eng.*, vol. 8, no. 4, 1996, doi: 10.1061/(asce)0899-1561(1996)8:4(189).

565 [19] J. Outinen and P. Mäkeläinen, “Mechanical properties of structural steel at elevated temperatures
566 and after cooling down,” *Fire Mater.*, vol. 28, no. 2–4, pp. 237–251, 2004, doi: 10.1002/fam.849.
567 [20] A. Y. Elghazouli, K. A. Cashell, and B. A. Izzuddin, “Experimental evaluation of the mechanical
568 properties of steel reinforcement at elevated temperature,” *Fire Saf. J.*, vol. 44, no. 6, pp. 909–
569 919, Aug. 2009, doi: 10.1016/j.firesaf.2009.05.004.
570 [21] R. Felicetti, P. G. Gambarova, and A. Meda, “Residual behavior of steel rebars and R/C sections
571 after a fire,” *Constr. Build. Mater.*, vol. 23, no. 12, pp. 3546–3555, Dec. 2009, doi:
572 10.1016/j.conbuildmat.2009.06.050.
573